Chapter 2

Foundations

2.1 Quantum calorimeter basics

The idea behind a quantum calorimeter is deceptively simple. A "calorimeter" is an instrument that measures energy,[1] and the word "quantum" refers to the fact that we are measuring the energy of quanta of light. Figure 2.1 is a schematic of the simplest calorimeter. An absorber with heat capacity C is connected via a weak link with thermal conductance G to a heat sink (also called a cold bath) at temperature T_b. If no power is applied, the absorber temperature $T(t)$ will be equal to the bath temperature. If a photon with energy E_γ is absorbed, then the temperature of the absorber will rise and then cool back to the bath temperature. The rise in temperature will be proportional to the energy of the photon ($\Delta T_\gamma = E_\gamma/C$). Thus by measuring the rise in temperature ΔT_γ as each photon comes in, the energy of the photons can be determined. That is quantum calorimetry in a nutshell.

If constant power is applied, then the absorber will rise to a temperature above the bath temperature until the power flowing into the absorber equals the power flowing out through the weak link into the cold bath. The thermal equation for this system is

$$C\frac{dT(t)}{dt} = P - P_\mathrm{link}\big(T(t), T_\mathrm{b}\big) + E_\gamma \delta(t - t_\gamma) \tag{2.1}$$

where P is the heat flow into the absorber[2], (which for now we are assuming constant or zero), and $P_\mathrm{link}\big(T(t), T_\mathrm{b}\big)$ is the power that flows from the absorber to the cold bath through the weak link. $E_\gamma \delta(t - t_\gamma)$ is an absorption event; the delta function deposition of the energy of photon γ into the absorber at time t_γ. The functional form of $P_\mathrm{link}\big(T(t), T_\mathrm{b}\big)$ depends on the physics of the particular device, and for now we will assume

$$P_\mathrm{link}\big(T(t), T_\mathrm{b}\big) = G\big(T(t) - T_\mathrm{b}\big) \tag{2.2}$$

[1] According to Webster, a calorimeter is "any of several apparatuses for measuring quantities of absorbed or evolved heat or for determining specific heats. From Latin *calor*."

[2] This power usually refers to the power dissipated by a thermometer with bias applied, but it could be radiation from the environment or any other parasitic load.

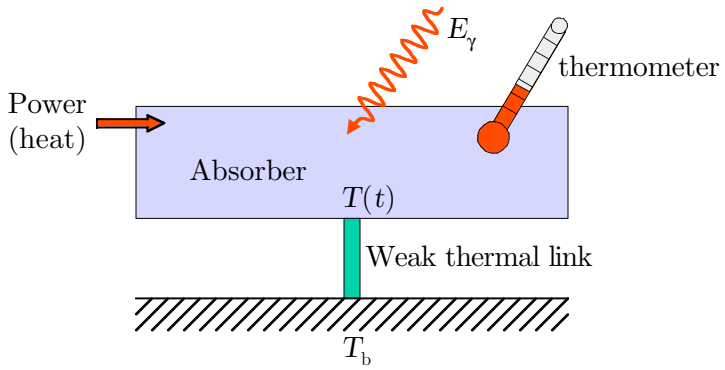

Figure 2.1: A simple calorimeter. An X-ray is absorbed in a pixel which has a weak thermal link to a cold bath. The pixel heats up when the X-ray deposits its energy in it, and then cools back down as heat flows from the pixel to the cold bath. This temperature pulse is measured by a thermometer. The height of the pulse is proportional to the energy of the X-ray.

which makes Eq. (2.1) linear, and taking $t_\gamma = 0$ we can immediately solve to obtain

$$T(t) = \frac{E_\gamma}{C} e^{-t/\tau_o} + \left(\frac{P}{G} + T_\mathrm{b}\right) \tag{2.3}$$

with a time constant $\tau_o \equiv C/G$ and a quiescent absorber temperature $P/G + T_\mathrm{b}$. So the simplest calorimeter has an exponential decay response with a time constant of C/G and an initial temperature rise $\Delta T_\gamma = E_\gamma/C$. By measuring $T(t)$ the energy and timing of incoming photons can be determined.

A bolometer is essentially the same device, but looking at many photons instead of one. The difference between a bolometer and a calorimeter is that the bolometer measures the power, usually from a flux of photons hitting the absorber in rapid succession, while a calorimeter usually measures the energy deposited by a single photon or particle.

For a basic overview of quantum calorimetry, see Stahle et al. (1999) or a more in depth treatment in Stahle (2000). For a general review of low temperature detectors and their applications, see Booth et al. (1996).

2.1.1 X-ray absorption and thermalization

In the calculation above we made the simplifying assumption that the photon thermalizes immediately into the absorber. Next, we briefly look at the process of absorption and thermalization.

In the 0.1 to 10 keV energy band (our band of interest for this thesis), the primary interactions of X-rays with matter are the photoelectric effect, Rayleigh scattering, and Compton scattering (Knoll, 1979). Rayleigh scattering is a coherent process where the X-ray is deflected off one of the atoms in the absorber. No energy is deposited in the absorber. Rayleigh scattering therefore does not produce any signal in our thermometer. In Compton

scattering, the X-ray scatters off an electron and imparts some of its energy to it. For X-rays in our energy band and the materials we use as absorbers, the cross section (probability to for the interaction to occur, see Knoll (1979), chap. 2) of Compton scattering is orders of magnitude less than for the photoelectric effect (Evans, 1955).

In the photoelectric effect, the X-ray is absorbed by an atom in the absorber, which ejects a previously bound electron with an energy $E_e = E_\gamma - E_b$, where E_γ is the X-ray energy and E_b is the binding energy of the electron to the atom. The binding energy of the electron must be lower than the energy of the X-ray. The most probable origin of the electron is the highest-energy bound state that satisfies the $E_b < E_\gamma$ condition. For absorbers like bismuth, rhenium and tin, X-rays in the 0.1 to 10 keV band will not have enough energy to kick off a K shell electron (see Center for X-ray optics; NIST physical reference data). L shell and higher bound electrons will be accessible depending on the material and the X-ray energy.

This ejected electron is called a "photoelectron." This photoelectron now has a much higher energy (E_e) than the average electron energy, and has a huge cross section with other electrons. The photoelectron's mean free path[3] is extremely short, and it collides with other electrons, shedding its energy. Also, the interaction of the X-ray with the atom leaves the atom with a vacancy in one of its bound shells. This vacancy is quickly filled by the capture of a free electron and/or the rearrangement of electrons from the other shells of the atom. In these processes one or more characteristic X-rays may be generated. In most cases these secondary X-rays are quickly reabsorbed close to the original site through photoelectric absorption with less tightly bound shells, and the process starts again. Another possibility is that the atom relaxes by the emission of an Auger electron. In this process, the excitation energy of the atom is transferred directly to one of its outer shell electrons, causing the electron to be ejected from the atom. This electron (called an Auger electron) appears with an energy given by the difference between the original atomic excitation energy and the binding energy of shell from which the electron was ejected. This process dominates for lower energy photoelectric absorption events and higher bound-shell vacancies.

Soon a ball of energetic electrons is created around the absorption point. As the number of electrons in this process increases, the average energy of any one electron goes down. As the mean electron energy goes down, electrons have a higher probability of releasing energy by the emission of phonons.[4] When the electron energy drops below a few eV, phonon emission becomes the dominant energy-loss mechanism. The mean free path increases as the energy of the particles decreases, so the size of the ball grows rapidly. Finally, the mean energy of all the particles in the detector rises and a Maxwell-Boltzman distribution

[3]The mean free path is the average distance a particle travels before hitting another particle, a quantity related to the cross section and the speed of the particle.

[4]In a perfect, infinite crystal made of atomic nuclei with their corresponding electrons that has been cooled to absolute zero, conduction band electrons propagating through the crystal would never collide with the nuclei. But no crystal is perfect or infinite or at absolute zero, and electrons do collide with the nuclei and excite the crystal vibrational modes. One can equivalently describe these vibrational modes by fundamental excitations called phonons. When we talk about phonons we are talking about the excited vibrational modes of the crystal. Ashcroft and Mermin (1976, chap. 23) gives a good description of phonons in the low-temperature limit.

around a higher mean energy is reached. This is what we call "thermalization," because the increase in mean energy is detected as an increase in the temperature of the detector.[5]

Cabrera et al. (1993) has done Monte-Carlo simulations and taken measurements on Si detectors to study these thermalization processes. Fann et al. (1993); Maris (1993); Tamura (1993) are other excellent papers on the subject.

2.2 Transition-edge sensors

Many methods of measuring the absorber temperature exist. Our group uses thermistors, i.e. resistive elements whose resistance is a function of temperature. This work is based on superconducting-Transition-Edge Sensors (TESs), sometimes called Superconducting Phase Thermometers (SPTs). A TES is a superconducting film operated in its superconducting transition (Figure 2.2). Since the R vs. T curve is very steep at the TES operation point, a small change in temperature causes a large change in resistance. Hoevers (2002) gives a review of current TES efforts.

2.2.1 Electrothermal feedback and pulse decay time

Several different ways of maintaining the TES in its transition have been developed (Galeazzi, 1998; Irwin, 1995b; Meier et al., 2000). We use the method developed by Irwin (1995b) called the electrothermal feedback TES (ETF-TES), and reproduce some of his theoretical results below. In this scheme the TES is voltage biased, and Joule heating of the TES maintains its temperature in the transition. The power input is a function of resistance $P(T) = V^2/R(T)$ and thus of temperature. Figure 2.2(b) shows the two power terms in Eq. (2.1) vs. temperature for the curve in Figure 2.2(a) and using typical values for the constants. When the TES is normal, the resistance is large, and the input power $P(T)$ is lower than the output power, so the TES cools. As it cools, it enters its transition, and the resistance rapidly decreases. As the resistance decreases, the input power $P(T)$ increases, slowing the cooling rate. The TES enters a stable equilibrium between the power leaving the device through the weak link and the power input through the Joule heating of the TES (the crossing point in the figure). If the temperature drops, the input power rapidly increases and heats the device back to the bias point. This is called negative ETF. The negative ETF makes the TES a self-biasing device which is very stable and easy to operate. As we shall see, the large negative slope of the output power curve that results from ETF also causes the pulses to decay more quickly, an added benefit which allows for devices with very high count rates. We will now derive the pulse decay time ($\tau_{\rm eff}$) and demonstrate its dependence on the device parameters.

[5] Electron-phonon decoupling at low energies produces an out of equilibrium electron temperature which is higher than the phonon temperature for 100's of μsec (Roukes et al., 1985). In our transition-edge sensors we measure the electron temperature.

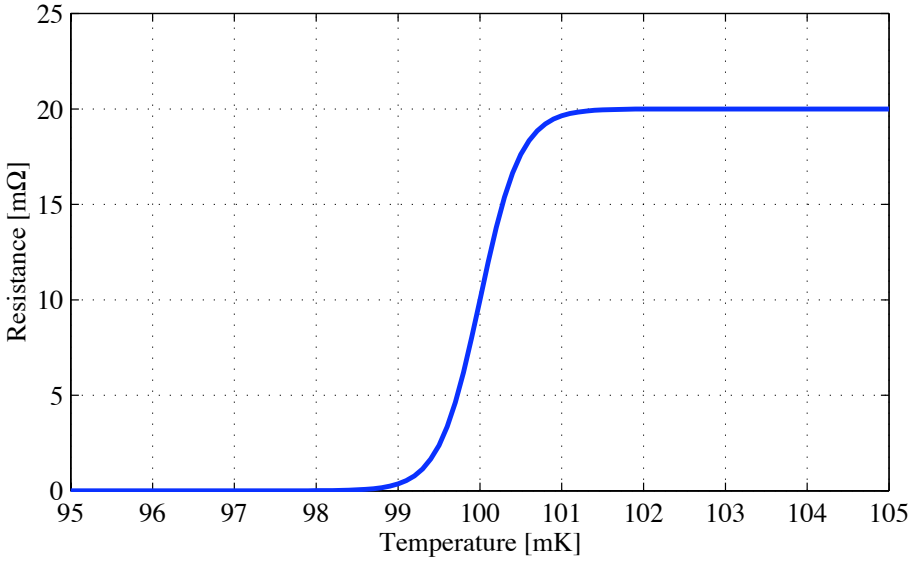

(a) Schematic of R vs. T curve for a transition-edge sensor. A TES is a superconducting film biased within its transition. Within the transition, a small temperature change creates a large change in the resistance, making a very sensitive thermometer within a small operating range.

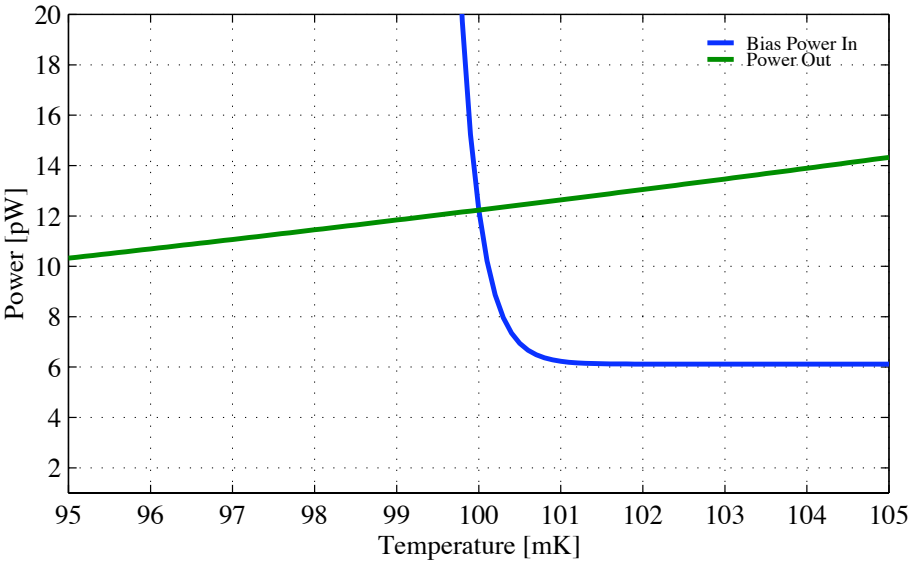

(b) Power into calorimeter at constant voltage V from bias $V^2/R(T)$ (at constant V) and power out of calorimeter through weak link as a function of temperature. The crossing point is the stable quiescent operating point of the TES. Notice the very sharp slope of the input power.

Figure 2.2: R and P vs. T for a TES

To gauge the sharpness of the transition, we define the dimensionless parameter α:

$$\alpha \equiv \frac{T}{R(T)}\frac{\partial R(T)}{\partial T} \tag{2.4}$$

where, for now, we have assumed that the resistance is only a function of temperature (it is also a function of current, but we will take that up in Chapter 3).

As we mentioned before, the functional form of the power output to the cold bath through the weak link depends on the physics of the weak link. In our devices the power output is of the form

$$P_{\rm link}\big(T(t), T_{\rm b}\big) = K\big(T(t)^n - T_{\rm b}^n\big) \tag{2.5}$$

where K is a constant and n is a number between 2 and 5 depending on the dominant mechanism of heat transfer and the dimensionality of the link (Anghel et al. 1998; Ashcroft and Mermin 1976, chap. 25).

Rewriting the thermal equation (Eq. (2.1)) we obtain

$$C\frac{dT(t)}{dt} = \frac{V^2}{R(T)} - K\big(T(t)^n - T_{\rm b}^n\big) + E_\gamma\delta(t - t_\gamma) \tag{2.6}$$

where again $E_\gamma\delta(t - t_\gamma)$ is a delta function input of energy E_γ at time t_γ, i.e. a photon. In quiescence

$$P = \frac{V^2}{R} = K(T^n - T_{\rm b}^n) \tag{2.7}$$

where P is the input power at a particular bias V.[6] To solve this non-linear differential equation analytically we must linearize the system. Using Taylor expansion (the procedure is explained in Section 3.1.1), we expand to first order in ΔT:

$$C\Delta\dot{T}(t) = \frac{V^2}{R} - K(T^n - T_{\rm b}^n) - \frac{V^2}{R^2}\frac{\partial R}{\partial T}\Delta T - nKT^{n-1}\Delta T + E_\gamma\delta(t - t_\gamma) \tag{2.8}$$

where R and T are the quiescent values and ΔT is the dynamic variable. Then from Eq. (2.7) the first two terms cancel. We define

$$G \equiv \frac{dP}{dT} = nKT^{n-1} \tag{2.9}$$

[6] Since we are operating in the transition of the TES, the change in temperature as R goes from zero to $R_{\rm n}$ can be very small. If we assume that $T = T_{\rm c}$ (where $T_{\rm c}$ is the critical superconducting transition temperature) for all points in the transition, then the quiescent power will be the same for any bias. Note that we are referring to the quiescent value of the power. This is reflected in the almost horizontal slope of the output power in Figure 2.2(b). The bias point is the intersection of the two lines.

set $P = V^2/R$, and use Eq. (2.4) to arrive at

$$\Delta\dot{T}(t) = -\left(\frac{\alpha P}{TC} + \frac{G}{C}\right)\Delta T + \frac{E_\gamma}{C}\delta(t - t_\gamma) \tag{2.10}$$

The solution to this equation as before is a simple exponential, but the effective time constant is now

$$\tau_{\text{eff}} = \frac{\tau_o}{1 + \frac{\alpha P}{TG}} \tag{2.11}$$

Substituting the definitions above for P and G and using Eq. (2.7) we get the equivalent

$$\tau_{\text{eff}} = \frac{\tau_o}{1 + \frac{\alpha}{n}\left(1 - \frac{T_{\text{b}}^n}{T^n}\right)} = \frac{\tau_o}{1 + \frac{\alpha\phi}{n}} \tag{2.12}$$

where

$$\phi \equiv \left(1 - \frac{T_{\text{b}}^n}{T^n}\right) \tag{2.13}$$

so ϕ goes from 1 to 0 as the bath temperature increases from absolute zero to the detector temperature. With this nomenclature the variables are the operating temperature and the base temperature; α and n can be determined from theory or more commonly from fitting data for each device. To keep the derivations general we will resort to the $\alpha\phi/n$ notation sparingly.

Defining "extreme electrothermal feedback regime" as a state where $T^n \gg T_{\text{b}}^n$ and $\alpha/n \gg 1$ we can express the decay time as

$$\tau_{\text{eff}} = \frac{n\tau_o}{\alpha} \tag{2.14}$$

For large α, ETF can thus make TES calorimeters have much faster decay times than their intrinsic time constants. We will see in the next section why it is desirable to have fast decay times. Looking at Eq. (2.11), one could argue that if one had a device with $\alpha \sim 5$ (as in semiconductors), one could just increase G to decrease τ_o to get the desired decay time. This is true, but in practice non-linear effects make it hard to achieve the same decay times in semiconductor calorimeters that are found in TES calorimeters. The main problem is power. As one increases G, one needs to increase the power into the thermistor (per Eq. (2.7)) to keep the thermistor at its same operating point. In both semiconductor and TES detectors, non-linear effects prevent the arbitrary increase of the input power. So once this limit has been reached, increasing α is the only way to make the decay time faster.

A note to the reader: this discussion is valid only for ETF calorimeters and assuming each X-ray is recorded for several decay-time constants after the peak (as explained in the next sections). Other bias techniques or other filtering methods that record only to slightly after the peak have different constraints and trade-offs. One must take great care when

comparing across these methods, since one must look at count rate, dead time, and energy resolution simultaneously.

2.2.2 Decay time and pile-up

To understand the importance of pulse decay time, we must talk about count rate, pile-up, dead time, and energy resolution. Count rate is the number of X-rays per unit time that hit the detector. Pile-up is the condition where an X-ray hits the detector, and while the detector is still recovering from the increase in temperature imparted by this first X-ray, a second X-ray hits. In a temperature vs. time plot, one sees the second X-ray on the "tail" of the first. Dead time is the percentage of time the detector is unusable while operating.

As we will discuss in more detail in Sections 2.3 and 3.1.5, the best energy resolution attainable by a calorimeter depends on various factors. One of these factors is bandwidth. Bandwidth is the width in frequency space over which the signal-to-noise ratio (See Section 3.1.3) is greater than some fiducial number, which we will take as 1. To get the high energy resolution desired, we must record the time evolution of an X-ray event to several times the decay time constant of the device. The longer we record the data, the larger our bandwidth becomes. Of course, there is an obvious reason for not making these records arbitrarily long: other X-rays will hit the detector. We want to make detectors that can handle a large count rate of X-rays. This is where decay time comes in. The faster the decay time, the less total time we need to record a particular pulse before we are ready for the next one. Pile-up occurs when an X-ray hits the detector while we are still recording the previous one. More complex algorithms must be used to untangle both photons and determine their respective energies. These algorithms generally degrade the achievable resolution. Every time this happens those two X-rays get a medium- or low-energy-resolution energy estimate, and cannot be counted in the high-energy resolution histogram. The percentage of time this happens accrues as dead time. We will discuss the other side of our bandwidth window (the high frequency side) and its effect on energy resolution in Section 2.3.1.

Photon emission is a stochastic process. We can determine what the *average* count rate in the detector is, but it is not possible to know *a priori* the time between any two consecutive events. The time could be long, or two photons could arrive almost simultaneously. So for any decay time and X-ray count rate there is pile-up. As the count rate or decay time goes down, pile-up becomes a rare event. The relation between pile-up and dead time, for a given count rate and decay time, obeys Poisson statistics and one must take these into account when designing a detector.

2.2.3 Stability condition

The temperature evolution after a photon is absorbed at $t_\gamma = 0$ is

$$\Delta T(t) = \frac{E_\gamma}{C} e^{-t/\tau_{\text{eff}}} \tag{2.15}$$

Using the definition of α and $\Delta I = -\frac{V}{R^2}\frac{\partial R}{\partial T}\Delta T$ we obtain the relation between current and temperature[7]

$$\Delta I = -\frac{\alpha I}{T}\Delta T \tag{2.16}$$

Thus the current will follow the equation

$$\begin{aligned}\Delta I(t) &= -\frac{\alpha I}{T}\frac{E_\gamma}{C}e^{-t/\tau_{\text{eff}}} \\ &= -\left(\frac{1}{\tau_{\text{eff}}} - \frac{1}{\tau_o}\right)\frac{E_\gamma}{V}e^{-t/\tau_{\text{eff}}} \\ &= \Delta I_{\text{meas}}e^{-t/\tau_{\text{eff}}}\end{aligned} \tag{2.17}$$

where $\Delta I_{\text{meas}} = -\frac{E_\gamma}{C}\frac{\alpha I}{T}$ is the initial drop in current measured from the resulting increase in resistance after the photon was absorbed.

Looking at Eq. (2.17) we see that for the current signal to be a decaying exponential, τ_{eff} has to be a positive number. From Eq. (2.11) we see that τ_{eff} will be as long as

$$\frac{\alpha P}{TG} > -1 \tag{2.18}$$

This equation defines the stability condition for this simple TES. Since P, G, and T are always positive, the only way that expression can be negative is to have a negative α. The sign of α depends on the slope of the R vs. T curve. For TESs, the slope is positive and so is α. For silicon thermistors, the resistance increases as the temperature decreases, so α is *negative* for these devices (a typical value is $\alpha = -5$). This is why TESs are voltage biased and silicon thermistors are current biased. *Negative* ETF will occur for voltage-biased positive-α and current-biased negative-α thermistors.

It is interesting to note that the crossover between stable and unstable (positive and negative τ_{eff}) does *not* occur when $\alpha = 0$, rather when $\alpha P/T = -G$. This effect can be explained by looking at the energy flow in the calorimeter. To set up this explanation let us take a short detour for another look at electrothermal feedback.

2.2.4 ETF revisited

Consider the calorimeter in Figure 2.1. In the steady state, with no noise sources (which we will talk about in Section 2.3), and no incident radiation, there are only two ways for energy to come in or go out of the calorimeter: through Joule heating of the thermistor, or through the weak link to the cold bath. The weak link to the cold bath is always there, and is a "pipe" through which any excess heat in the calorimeter will be siphoned away with a time constant $\tau_o = C/G$.

[7] Eq. (2.16) is valid only for perfect voltage bias and a resistance curve that is only a function of temperature. See Section 3.1.1, Eq. (3.16).

If one turns the current through the thermistor off, the Joule power will be zero, and the quiescent temperature of the calorimeter will be the same as the cold bath temperature; $T = T_\mathrm{b}$. A photon incident on the calorimeter will heat it up to a temperature $T_\mathrm{b} + E_\gamma/C$, and consequently this heat will be released into the cold bath with a decaying exponential form with a time constant of τ_o.

Now we turn the voltage across the thermistor on. The Joule power heats the calorimeter, and it comes to a stable equilibrium at some temperature $T > T_\mathrm{b}$. As can be seen on Figure 2.2(b), the Joule power dissipated in the TES is much larger than the power leaking to the weak link into the cold bath for $T < 100$ mK, and the reverse for $T > 100$ mK. The TES is stable only at $T = 100$ mK ($T_\mathrm{b} = 50$ mK in the model used for the figure). Now a photon is absorbed and heats the calorimeter to a temperature $T + E_\gamma/C$. Since the temperature is higher than T, we see in Figure 2.2(b) that the Joule power drops. From Eq. (2.10) we see that the term $\alpha P/T$ has the same units as thermal conductance, and comes into the equation in the same place as G. In fact, these two terms act as two thermal conductances in parallel, one real (the cold bath siphoning heat out of the calorimeter through the weak link), and one *virtual* (the electrical circuit *siphoning heat* out of the calorimeter by reducing the amount it put in). We can then make the definitions

$$G_\mathrm{ETF} \equiv \frac{\alpha P}{T} \qquad\qquad \tau_\mathrm{ETF} \equiv \frac{C}{G_\mathrm{ETF}} = \frac{C}{\frac{\alpha P}{T}} = \frac{\alpha P}{TG}\tau_o \tag{2.19}$$

G and G_ETF added in parallel give an effective ETF thermal conductance out of the calorimeter of $G_\mathrm{eff} = G + \alpha P/T$, for an effective time constant of

$$\tau_\mathrm{eff} = \frac{C}{G_\mathrm{eff}} = \frac{C}{G + G_\mathrm{ETF}} = \frac{C/G}{1 + \frac{\alpha P}{TG}} = \frac{1}{\frac{1}{\tau_o} + \frac{1}{\tau_\mathrm{ETF}}} \tag{2.20}$$

Now it is clear why ETF speeds up pulses. In extreme ETF, the "conductance" $G_\mathrm{ETF} = \alpha P/T \gg G$ and so dominates the effective time constant; in extreme ETF, $\tau_\mathrm{eff} \to \tau_\mathrm{ETF}$.

In fact, any power source applied to the calorimeter that is fed back (turned down in response to a pulse) will act as a virtual conductance and exhibit this speed-up behavior. Various techniques have been proposed and implemented to substitute or augment ETF (Galeazzi, 1998; Meier et al., 2000; Nam et al., 1999). The advantages and disadvantages of these other techniques need to be properly assessed.

It is now easy to see why the calorimeter stability point is not when $\alpha = 0$. Under voltage bias, when α is negative, the system is in positive feedback. For $\alpha < 0$, $\alpha P/T$ is not a conductance siphoning out heat, but a pipe pumping it in, in proportion to an excitation ΔT. But as long as $|\alpha|P/T < G$, the heat can go out through G faster than it can get in through $\alpha T/P$, and the calorimeter is stable (although for this regime where $\alpha < 0$ and the calorimeter is still stable the time constant $\tau_\mathrm{eff} > \tau_o$). In other words, as long as Eq. (2.18) holds, a device in positive feedback (negative G_ETF) will still be stable. If $\alpha P/T < G$, then the positive feedback puts more power in the calorimeter than what goes out to the cold bath through the conductance G, and the TES will heat up and "latch" at the normal resistance R_n.

Actually, when the TES is unstable, positive feedback will make the TES run away in whatever direction a small perturbation takes it from the quiescent temperature. So if a little dip in temperature occurs, the positive ETF will shut the power down and the TES will "latch" at $R = 0$. Whether it goes to $R = 0$ or $R = R_{\rm n}$ just depends on the initial perturbation, the important thing is that if the stability condition is not met, the TES is unusable as a thermometer.

2.2.5 Energy integral

Since $\Delta P(t) = V\Delta I(t)$ for constant voltage bias, we can integrate the current to obtain the total energy removed from the system from the reduction in Joule power,[8] which will be

$$E_{\rm Joule} = -\tau_{\rm eff} V \Delta I_{\rm meas} = -\frac{1}{1+\frac{TG}{\alpha P}} E_\gamma \tag{2.21}$$

$$= -\frac{1}{1+\frac{n}{\alpha\phi}} E_\gamma \tag{2.22}$$

$$= -\left(1 - \frac{\tau_{\rm eff}}{\tau_o}\right) E_\gamma \tag{2.23}$$

As we can see, the decrease in Joule power does not integrate to the energy of the photon for low values of α, but approaches that value as one moves into the extreme ETF regime, where $\tau_{\rm eff} \to 0$. For a detector with an α of 100 (representative or our current TESs), with $n = 4$ and $\phi \sim 1$, $E_{\rm Joule} = 0.96E_\gamma$. For a detector with $\alpha = 5$ (representative of our current silicon thermistors), $E_{\rm Joule} = 0.56E_\gamma$. Note that this derivation assumes perfect voltage bias and a resistance function that does not depend on current. Both these factors change the measured energy, and we show that derivation in Section 3.1.1.

Finally, we point out that we are assuming that all the energy of the photon is deposited and thermalizes in the TES, i.e., the thermalization efficiency is 1. If a fraction of the energy of each photon is not thermalized, then this energy will not be measured, and one must multiply the above E_γ by the thermalization efficiency to get the correct $E_{\rm Joule}$. The loss mechanism is usually due to hot electron or hot phonon effects which make the thermalization of the absorber non-ideal. For example, Miller (2001) finds the Stanford optical tungsten TESs have a thermalization efficiency of 42% due to phonon losses to the substrate.

2.2.6 Saturation in a TES

A TES is a very sensitive thermometer, but it only operates within a finite range of temperatures. This range is dictated by the width of the transition of the TES. In Figure 2.2(a) the total transition width is about 1.5 mK. The linear portion is roughly 0.5 mK. If the transition were wider, we would have a larger operating range, but at the same time the gain of our thermistor would decrease, as the slope of the R vs. T curve decreases.

[8] This is basically the amount of energy siphoned by $G_{\rm ETF}$.

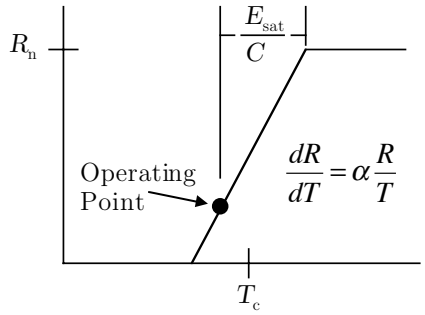

Figure 2.3: Assumed R vs. T curve for this thesis. $\Delta T_{\rm sat} = E_{\rm sat}/C$ only for the single-pixel TES.

In a linear model, the resistance vs. temperature function is a straight line, with the slope determined by $\alpha\frac{R}{T}$ evaluated at the steady state point of the real curve (Figure 2.2(a)). For the purposes of this thesis, we will model the R-T curve as in Figure 2.3. The curve is a straight line from zero to $R_{\rm n}$ and then abruptly becomes horizontal.

We define *saturation energy* as the photon energy that causes any TES in a calorimeter to have a temperature swing large enough that its resistance reaches $R_{\rm n}$. For a single pixel calorimeter without a decoupled absorber, this energy is

$$E_{\rm sat} = C\Delta T_{\rm sat} \tag{2.24}$$

where $\Delta T_{\rm sat}$ is the maximum temperature excursion from the operating point that is still in the linear range. From the definition of α, we can rewrite this as

$$E_{\rm sat} = \frac{C}{\alpha}\frac{\Delta R_{\rm sat}}{R}T \tag{2.25}$$

If we assume we bias the device in the middle of its transition, then $R = \Delta R_{\rm sat} = R_{\rm n}/2$, and $T = T_{\rm c}$. We then have

$$E_{\rm sat} \approx \frac{C}{\alpha}T_{\rm c} \tag{2.26}$$

For any application, there is always a desired energy range one wants the detector to operate in. The maximum energy one needs to be able to resolve determines $E_{\rm sat}$. This in turn places constraints on the value of C, α and $T_{\rm c}$. This saturation energy has direct implications on the ultimate resolution of a TES, since (as we will see in the next section) the theoretical resolution is a function of all these variables:

$$\Delta E_{\rm rms} \propto \sqrt{\frac{C}{\alpha}T^2} \propto \sqrt{E_{\rm sat}} \tag{2.27}$$

For Part I of this thesis, we will assume $\Delta T_{\rm sat} = 0.5$ mK, and since we are interested in X-ray detectors, we will use an $E_{\rm sat} = 6$ keV, which means $C = 1.92$ pJ/K (using Eq. (2.24)).

We will use 0.5 mK as the fiducial value of $\Delta T_{\rm sat}$ for our single-pixel TES benchmarks, and keep the overall temperature excursion of the position-sensitive TESs to this number. There is nothing magical about 0.5 mK, we just need a yard stick to define saturation and that value is consistent with our current data. Note that if this value for the heat capacity is used in Eq. (2.26), with a 6 keV saturation energy and a critical temperature of 75 mK, we obtain an α of 150. For this thesis we will use a more conservative α of 90, which is more consistent with our data. Eq. (2.26) does not take into account the curvature of the real R vs. T curves, which are not as steep near saturation as in the middle of the transition. We will use Eq. (2.24) as our saturation condition.

There is a very important point that must be made here. The limiting factor for the amount of energy the calorimeter can absorb and stay linear is the maximum change in temperature that the *thermistor* incurs. In designs where the absorber is decoupled by a thermal link from the thermistor, the initial rise in temperature of the absorber will be $E/C_{\rm abs}$, but the temperature rise of the thermistor will depend on the strength of the thermal link (in the limit of a very weak thermal link, the thermistor's temperature change tends toward zero, and it acts as a bolometer). The problem is that the moment one decouples the absorber from the thermistor, a phonon noise term due to this link enters the equations, and worsens the energy resolution. But since a calorimeter cannot be fully described by an energy resolution at a single energy, there are trade-offs to be made between dynamic range, energy resolution at a particular energy of interest, and the energy resolution as a function of energy. The non-linearities and range of operating and analysis modes encountered when pushing the dynamic-range/energy-resolution envelope do not allow for a succinct final answer. We will be looking at detectors with low heat capacities in which we are able to see high energy X-rays because of the weak coupling between the absorbers and the TESs. We will discuss this in Chapter 7. The noise from a decoupled absorber is discussed in Appendix A.

2.3 Single-pixel energy resolution

To understand the energy resolution of a calorimeter, we will look at simple model of a single-pixel thermistor calorimeter where all amplifier and other external noise sources are assumed to be small enough to be negligible. In this case, we only have two sources of noise: the Johnson noise from the resistor, and phonon noise from the connection to the cold bath.

Phonon noise is the thermodynamic power fluctuations through the thermal conductance G connecting the calorimeter to the cold bath. These power fluctuations create temperature fluctuations in the calorimeter. The heat capacity of the calorimeter and how well it is coupled to the cold bath through the conductance G give the system its characteristic time constant $\tau_o = C/G$. This time constant is the decay time of a simple calorimeter with no feedback. It is also the time constant that determines how fast the calorimeter can change its temperature. Although the power fluctuations are fairly flat at all frequencies of interest, the response of the calorimeter is not. Temperature fluctuations faster than the frequency $\sim 1/2\pi\tau_o$ are damped, so the spectrum of the temperature fluctuations has a -3 dB point

(a 1 pole roll-off) at $1/2\pi\tau_o$.

Johnson noise is the voltage fluctuations across any resistor due to the Brownian motion of the electrons in the resistor. The frequency distribution of these fluctuations is white for all frequencies of interest. These voltage fluctuations cause a change in the measured resistance of the TES, and so become a source of noise.

The full calorimeter theory will be presented in Chapter 3, so we will just show some of the general trends here. With these two sources of noise, the energy resolution of a calorimeter in the limit where $\alpha P/TG \gg 1$ can be expressed as (Irwin, 1995b):

$$\Delta E_{\mathrm{FWHM}} = 2.355 \times \sqrt{4k_{\mathrm{B}}T^2C\frac{1}{\alpha}\sqrt{\frac{n}{2}}} \tag{2.28}$$

where k_{B} is Boltzman's constant, T is the quiescent calorimeter temperature, C is the heat capacity, α is defined in Eq. (2.4), and n is the exponent in Eq. (2.7). See Eq. (3.75) for a more general expression of the energy the resolution.

Looking at the current signal for a pulse in Eq. (2.17) we see in the first line of that equation that the signal is proportional to α. Figure 2.4(a) shows a frequency power spectrum of a photon hit (the signal) and the noise terms on a set of calorimeters with progressively larger α. No electrothermal feedback has been applied to allow the intrinsic behavior to be seen. For $\alpha = 1$, both the signal and the phonon noise are below the horizontal Johnson noise level. As α increases, the signal gets bigger and rises above the Johnson noise. The "knee" of the curve occurs at the same frequency; without ETF, increasing α increases the size of the signal but does not speed up the pulses. A measure of the energy resolution can be made by looking at the signal-to-noise ratio (*SNR*). An quick estimate of the *SNR* can be made by looking at how much area there is between the signal and the noise. As α increases, even though the phonon noise increases along with the signal the *SNR* increases. Eq. (2.28) shows that the energy resolution indeed gets better (smaller ΔE) for higher α.

Figure 2.4(b) shows the same set of calorimeters, but with ETF turned on. There are two effects. First, pulse speed-up. Extreme ETF causes $\tau_{\mathrm{eff}} \rightarrow \tau_{\mathrm{ETF}} = C/G_{\mathrm{ETF}} \simeq nC/\alpha G$. So as α increases, the "knee" (at $1/2\pi\tau_{\mathrm{eff}}$) occurs at higher and higher frequencies. The second effect of ETF is to suppress all curves below $1/2\pi\tau_{\mathrm{eff}}$. Note that for each α, the amount suppressed in the signal, the Johnson noise and the phonon noise is the same, so the *SNR* for the ETF curves is identical to that for the respective no-ETF curves. We will see in Section 3.1.3 that this means the amount of ETF does *not* affect the resolution of a calorimeter. It *does* change the decay time τ_{eff}.

If one had a device with an α of 10, one could try to obtain the same fast decay times of the higher α devices by increasing G. Figure 2.5(a) shows a no-ETF plot of an $\alpha = 10$ device at different values of G. The "knee" goes out in frequency, but note that per Eq. (2.7) the power into the calorimeter must also increase as G increases to maintain the device in the same place in its transition. The effect of this necessary increase in power is that the energy resolution does not change. Thus, for all the curves in Figure 2.5 the resolution is 5 eV, just like the $\alpha = 10$ device in Figure 2.4.

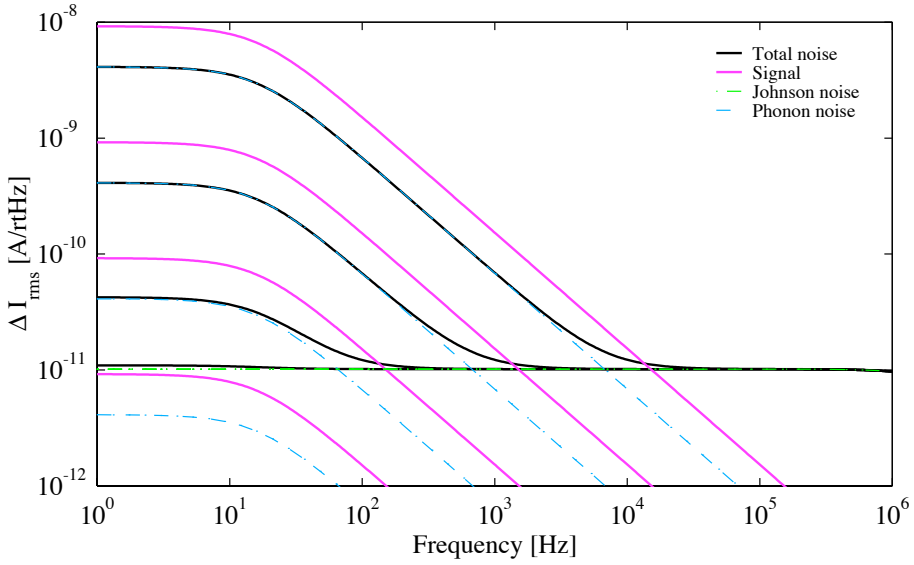

(a) No ETF

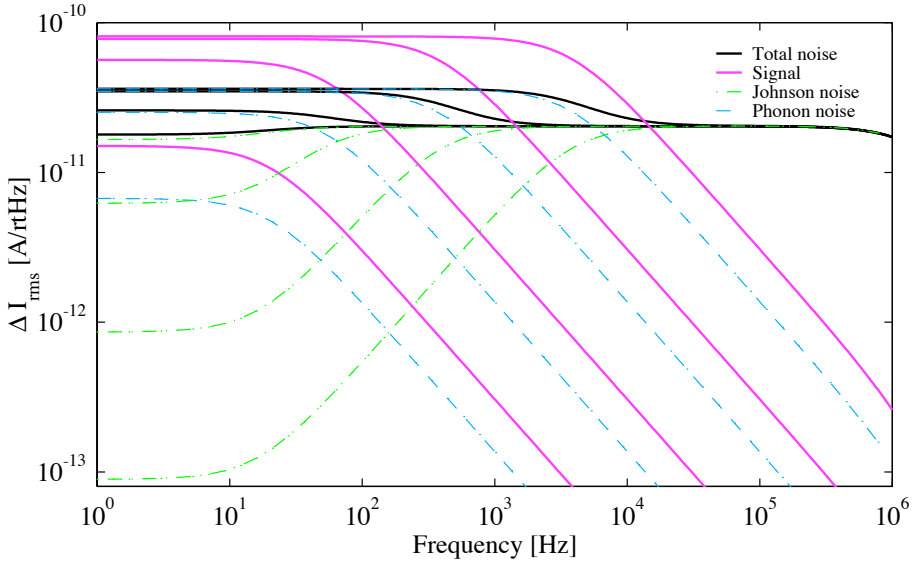

(b) With ETF

Figure 2.4: Current noise for α of 1, 10, 100, and 1000. The lowest magnitude curves correspond to $\alpha = 1$, and the largest to $\alpha = 1000$. The energy resolution in each case is 25, 5, 1.5, and 0.5 eV, respectively.

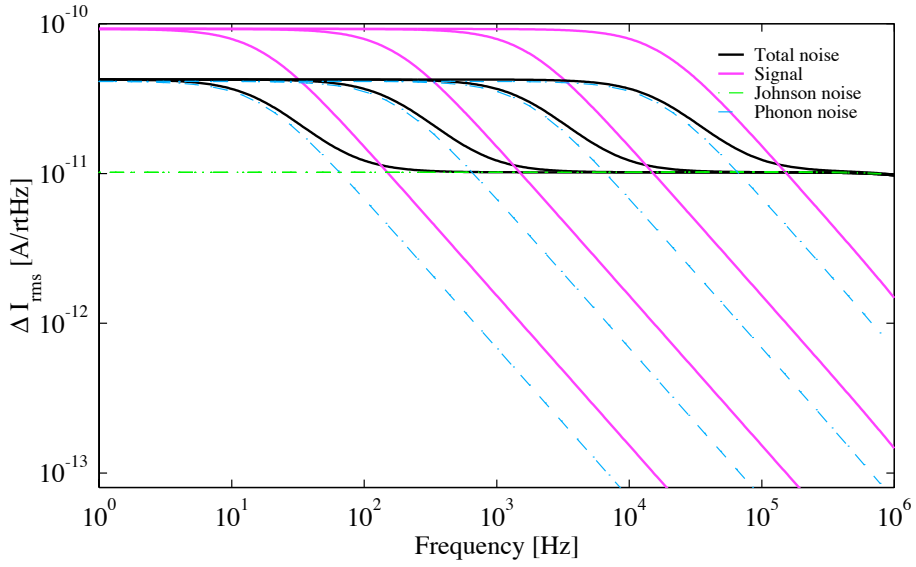

(a) No ETF

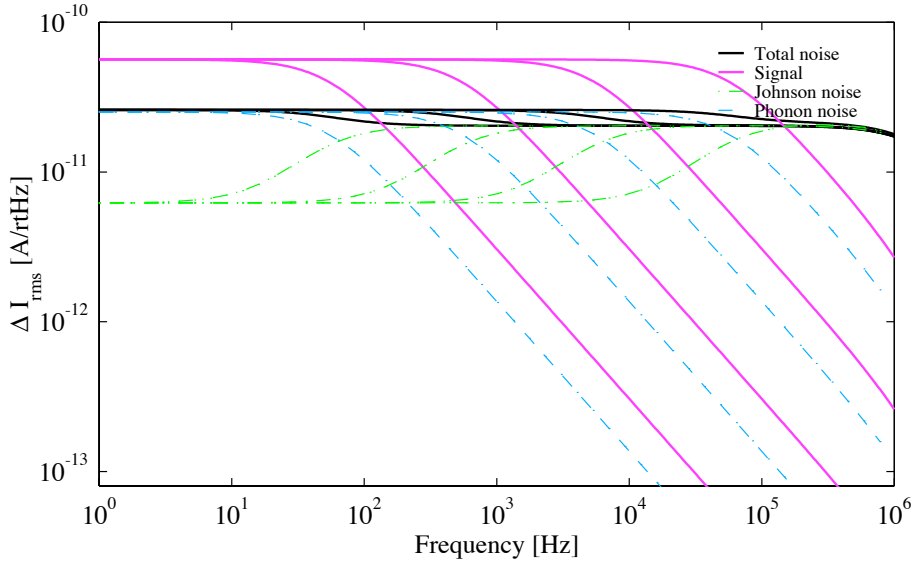

(b) With ETF

Figure 2.5: Current noise for $\alpha = 10$, conductance of G, $10G$, $100G$, $1000G$. The energy resolution for each case is 5 eV.

One might be tempted to think that the bigger the α the better, since one obtains better resolution. The problem in this argument has to do with saturation. Since α is a measure of the steepness of the transition, the bigger the α, the steeper the transition. In Section 2.2.6 we imposed a fiducial temperature excursion of 1/2 mK for a device with an α of 90. For each value of α, the temperature excursion to reach saturation and the heat capacity needed must be calculated. The result is that, for a maximum photon energy $E_{\rm sat}$ with which the detector reaches saturation, the ratio C/α remains the same. Using Eq. (2.26) we can rewrite the resolution as

$$\Delta E_{\rm FWHM} = 2.355 \times \sqrt{4k_{\rm B}TE_{\rm sat}\sqrt{\frac{n}{2}}} \tag{2.29}$$

So in the strong ETF limit, where Eq. (2.28) is valid, energy resolution is independent of α (for the same saturation energy). For the low α case, where one might not be in the strong ETF limit, Eq. (3.75) must be used. This is the case of silicon thermistors, whose value of α is ~ -5.

2.3.1 Energy resolution and thermalization

In Section 2.2.2 we discussed the need to have long integration times to get more bandwidth at the lower frequencies. Looking at Figure 2.4(b) for the case $\alpha = 100$, we see the signal rolls off at about 300 Hz. To get good energy resolution we would want to get to as low an energy as possible given the rate and pile-up constraints. Up to now we have been assuming that the thermalization takes place instantly, which makes the rise of the pulse instantaneous also. The Fourier transform of this perfect exponential is the signal curve shown in Figure 2.4(b). But in the real world, there is some thermalization time, due to the processes discussed in Section 2.1.1. This means the rise of the pulse is not instantaneous, but has a rise that can be modeled as a rising exponential. This will create a second roll off at a frequency $1/2\pi\tau_{\rm r}$ where $\tau_{\rm r}$ is the rise time constant. This roll off will make the signal cross over the noise at a lower frequency, lowering the bandwidth and thus reducing the energy resolution. If the thermalization time is fast enough that this roll off occurs at frequencies above the bandwidth imposed by the ideal signal and Johnson noise crossover, then the thermalization time does not affect the resolution since it is outside the defined bandwidth. Thus fast thermalization is important in single-pixel TESs.

As we will see in Section 2.4.1 and Section 4.5.1, for a PoST there is always some degradation in energy resolution from roll offs at high frequencies. The trick is to loose as little resolution as possible while still determining the position of the X-ray absorption in the PoST. We will discuss these issues in more detail next.

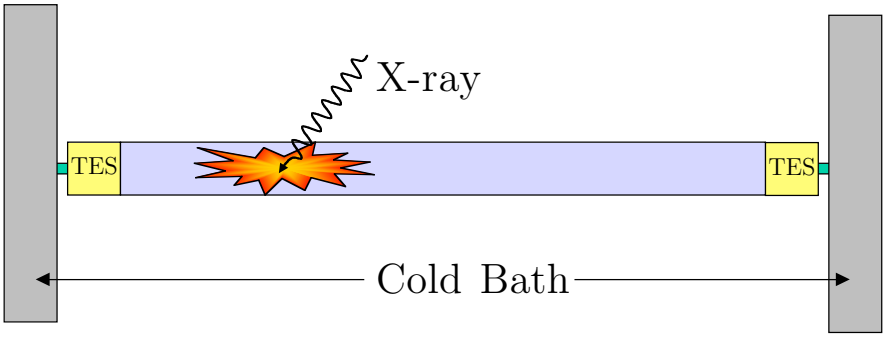

Figure 2.6: Concept for a one-dimensional imaging calorimeter. Two thermometers sense the same event, and the difference in signals provides the position information, while the pulse heights provide a measurement of the energy.

2.4 Position-sensitive calorimeters

As mentioned in Section 1.4 the current limiting factor to fabricating kilo-pixel calorimeter arrays is the available number of readout channels. Although great progress in SQUID multiplexing is being made (Chervenak et al., 1999), in the near future the total number of SQUID channels including multiplexing will be in the order of a few thousand. To increase the number of pixels another order of magnitude, we have developed the Position-Sensitive-TES (PoST) calorimeter.

In general, an imaging calorimeter uses one or more thermometers to analyze the signal produced by a photon absorption event in an absorber. For the same energy photons, the signal received by the thermometers varies in some detectable way depending on the position in the absorber where the event occurred. In other words, the absorber exhibits position dependence. If one can use the information in the signal shape to determine the location of photon absorption and the photon energy, one has an imaging calorimeter. This definition does not impose restrictions on the type of thermometer or absorber used, nor on the method of position or energy determination from the produced signal.

The imaging calorimeter can be a one-dimensional "strip" absorber with one or more thermometers, or a two-dimensional "plane" absorber with two or more thermometers. In this work we have concentrated on the simpler one-dimensional case, although the arguments put forth are equally valid for the two dimensional case, which we consider in Section 8.2.

Figure 2.6 shows a schematic of a one-dimensional position-sensitive calorimeter. The width of the PoST defines the pixel size in that direction, while the length-wise pixel size depends on how one bins the information from the detector and depends on the application. For example, Constellation-X detectors have a specified pixel size of 250 μm, so this would be the width of the PoST, while the number of pixels would be equal to the length of the absorber divided by 250 μm. When an X-ray event occurs, heat propagates down the absorber and reaches the thermometers. Since the PoST is connected to a cold heat sink,